Polymer Degradation and Stability 239 (2025) 111430

Contents lists available at ScienceDirect

Polymer Degradation and Stability

journal homepage: www.journals.elsevier.com/polymer-degradation-and-stability

α-amino acid-derived polyamidoamines as photostabilizers for cotton

Sofia Treccani, Jenny Alongi, Paolo Ferruti, Elisabetta Ranucci *

Dipartimento di Chimica, Università degli Studi di Milano, Via C. Golgi 19, 20133, Italy

ARTICLE INFO

Keywords:
Cotton
Cellulose
Photoaging
Photostabilizers
Polyamidoamines

ABSTRACT

Arginine- (M-ARG), glycine- (M-GLY), serine- (M-SER), histidine- (M-HIS) and tyrosine/arginine- (M-TYR_{30}-ARG_{70}) derived polyamidoamines (PAAs) were studied as cotton photostabilizers. Cotton strips with a 6 wt. % PAA add-on were subjected to accelerated photoaging in a solar chamber under UVA–UVB exposure at 40 % relative humidity and 30–35 °C. Colorimetric analysis was conducted at 15-minute intervals during irradiation. Virgin cotton exhibited significantly more yellowing than PAA-treated fabrics, except for those treated with M-TYR_{30}-ARG_{70}. Scanning electron microscopy revealed slight surface erosion on untreated cotton (COT) fibers after prolonged UV exposure, whereas PAA-treated cotton (COT/PAA) showed uniform PAA coatings with only minor surface wrinkles and localized fractures. Colorimetric analysis enabled ranking the photostability of COT/PAA samples as follows: COT/M-ARG > COT/M-GLY > COT/M-SER > COT/M-HIS > COT > COT/M-TYR_{30}-ARG_{70}. These results demonstrate that all PAAs enhanced UV protection, except for M-TYR_{30}-ARG_{70}. Nuclear magnetic resonance analysis of PAA coatings extracted from photoaged cotton showed no detectable structural degradation. The results confirm that α-amino acid-derived PAAs effectively protect cotton from photoaging, although formulations containing UVB-absorbing residues exhibit increased susceptibility to irradiation. The effectiveness of PAAs was attributed to the radical scavenging activity of tert-amine groups and the side-chain residues within their repeat units.

1. Introduction

UV irradiation is widely recognized for inducing photodegradation in cellulose by facilitating the formation of reactive peroxyl radicals and oxidized groups, such as hydroperoxides [1–4]. These species initiate chain reactions that result in material degradation and aging. The degradation process involves the decomposition of hydroperoxides into hydroxyl radicals. This occurs either under UV irradiation or through the catalytic activity of transition metal ions in their reduced form, such as Cu^{+} and Fe^{2+} [5,6]. UV exposure can introduce new functional groups, such as carbonyl and carboxyl groups, increasing the susceptibility of cellulose to degradation. Photoaging causes a deterioration in the physical and aesthetic properties of cellulosic materials, - paper, textiles, wood products - particularly when exposed to air under ambient conditions. This has significant implications for the preservation of cultural heritage and presents challenges in materials science, given the widespread use of cellulosic fibers in composites. Strategies to protect cellulose from photoaging include the incorporation of photostabilizers with various mechanisms of action, such as UV absorbers, reactive oxygen species (ROS) scavengers, and antioxidants. The use of UV absorbers is the most commercially exploited approach. The main UV absorbers currently on the market belong to the families of benzophenones, benzotriazoles, and triazines. Benzophenones, such as benzophenone-3 (BP-3, oxybenzone) and benzophenone-4 (BP-4, sulisobenzone), effectively absorb UV radiation. Specifically, BP-3 absorbs between 280 and 340 nm, (with absorption peaks around 288 nm and 325 nm), whereas BP-4 provides effective protection against UVB and short UVA rays. Some commercial examples are Chimassorb® 81, Uvinul® 3008 and Uvinul® 400. Benzotriazoles, including Tinuvin® P and Tinuvin® 327, provide protection across a broader UV spectrum (280–400 nm) in comparison with benzophenones. Triazines, such as Cyasorb UV-1164 and Cyasorb UV-3638, are recognized for their outstanding photostability and efficiency as UV absorbers, as well. From an overall consideration, BP-4 is the most common UV absorber for cotton and cellulosic fabrics, while triazines and benzotriazoles are preferred for technical and synthetic fabrics. Hindered amine light stabilizers (HALS) do not absorb UV radiation but function as radical scavengers during polymer photooxidation, thereby preventing cellulose degradation [7]. Benzophenones, benzotriazoles and triazines are often combined with HALS to exploit a synergistic action.

* Corresponding author.
E-mail address: elisabetta.ranucci@unimi.it (E. Ranucci).

https://doi.org/10.1016/j.polymdegradstab.2025.111430
Received 21 March 2025; Received in revised form 15 May 2025; Accepted 18 May 2025
Available online 20 May 2025

Table 1
Experimental conditions adopted in the synthesis of PAAs[a].

PAA	α-Amino acid	α-Amino acid (g; mmol)	$LiOH{\cdot}H_2O$ (g; mmol)	Temperature (°C)	Time (days)
M-ARG	Arginine	0.56; 3.2	–	50	9
M-GLY	Glycine	0.24; 3.2	0.14; 3.2	–	5
M-SER	Serine	0.34; 3.2	0.14; 3.2	–	5
M-HIS	Histidine	0.50; 3.2	0.14; 3.2	50	9
M- TYR_{30}-ARG_{70}	Arginine	0.40; 2.24	–	75	8
	Tyrosine	0.18; 0.96	0.04; 0.96		

[a] All preparations were performed using 0.50 g (3.2 mmol) N,N'-methylenebisacrylamide and 1.2 mL H_2O.

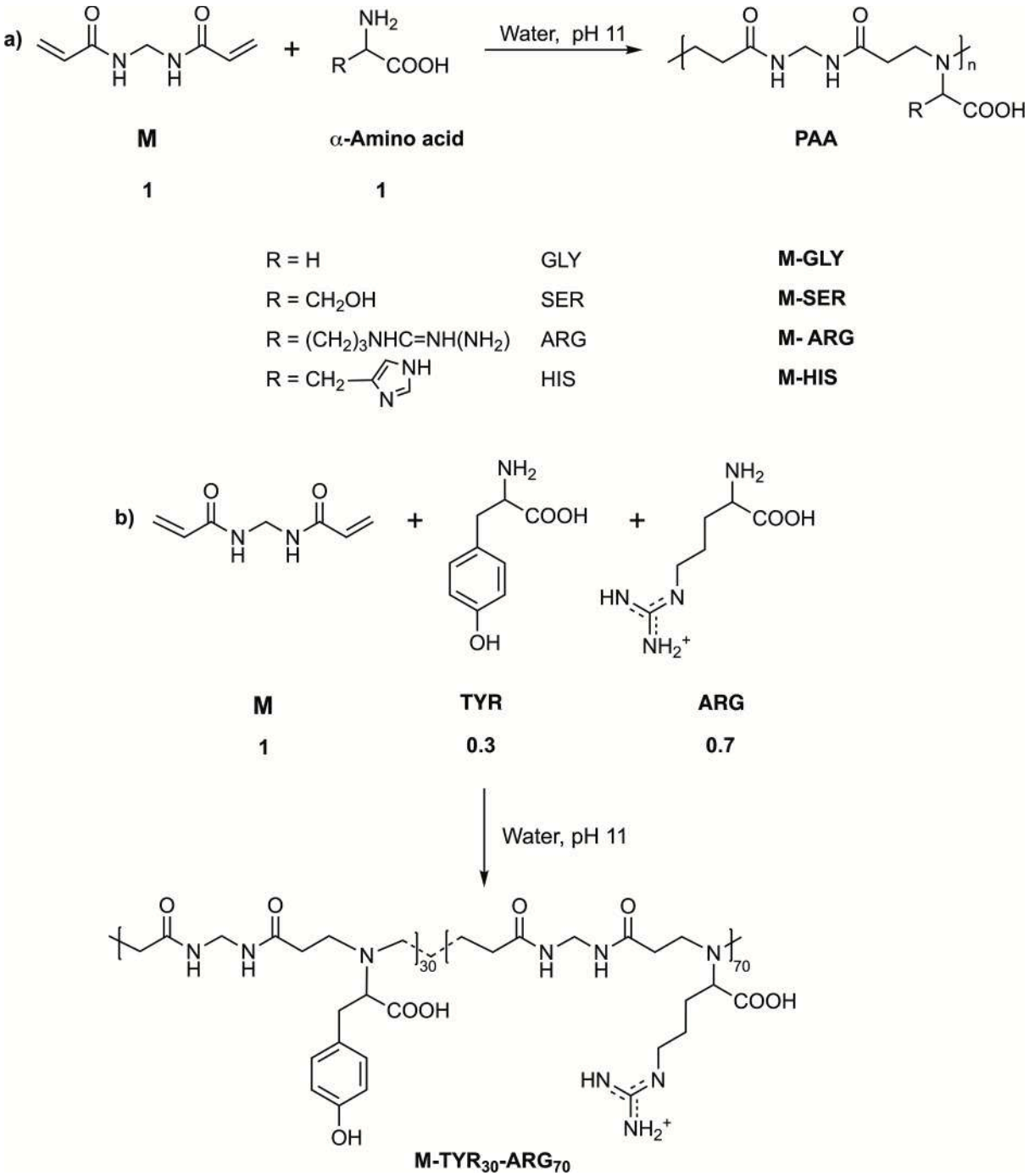

Scheme 1. Synthesis of PAA homopolymers (a) and of the tyrosine/arginine-based copolymer M-TYR_{30}-ARG_{70} (b). For the sake of simplicity, charges have been omitted.

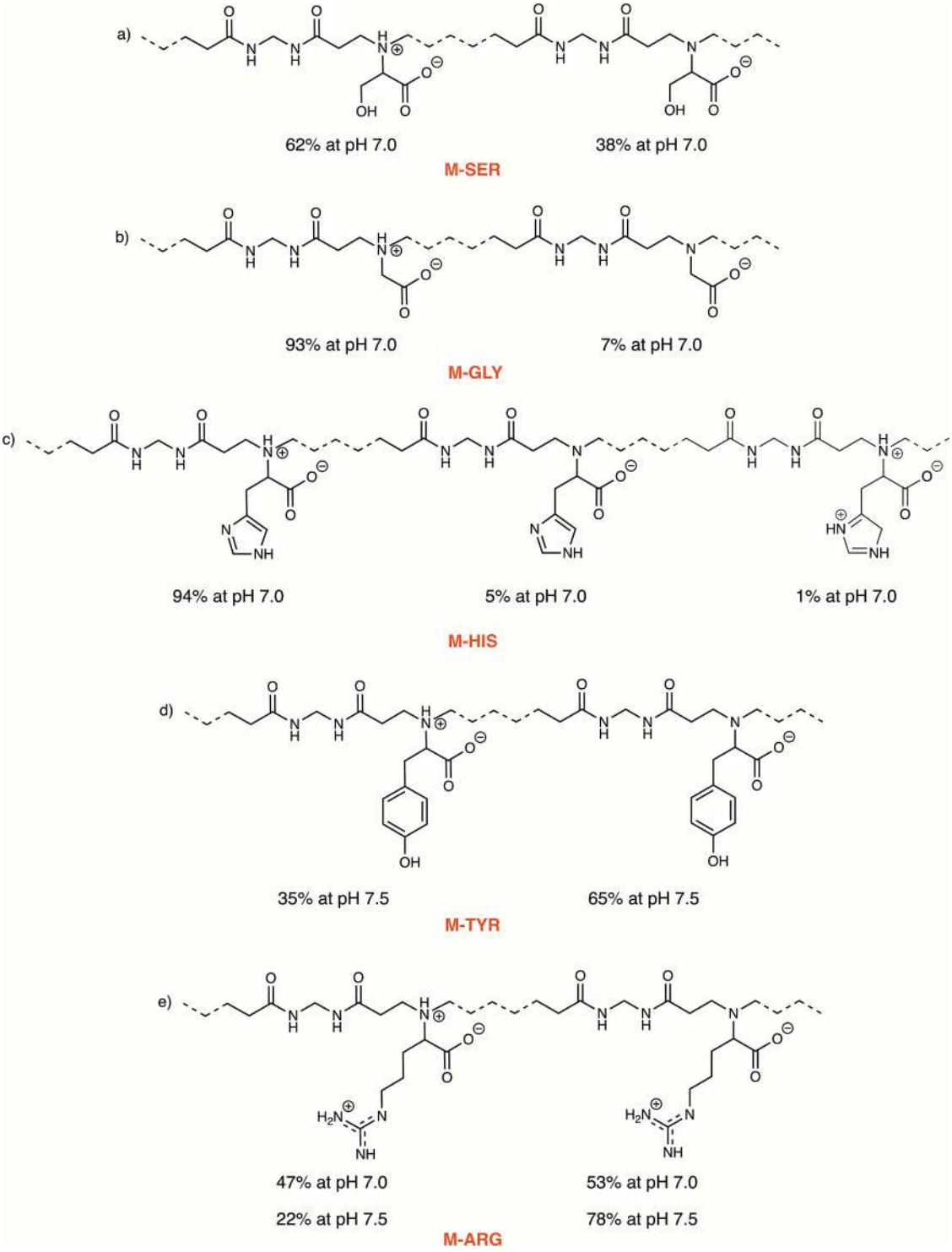

Fig. 1. Distribution of ionic species in PAA repeat units at pH 7.0 and, specifically for the M-TYR and M-ARG units, at pH 7.5.

Although UV absorbers effectively protect cellulose from UV-induced photoaging, they also have drawbacks and limitations that can impact their performance, environmental sustainability, and cost. Some benzophenones [8,9] and benzotriazoles [10,11] have been recognized as presenting potential health and environmental risks.

Designing UV stabilizers with environmental considerations for cellulosic materials is complex. Polymeric photostabilizers address this by exhibiting low volatility and solvent resistance, reducing leaching and improving the overall environmental and safety characteristics of the end products [12].

Polyamidoamines (PAAs) are synthetic polymers prepared by the aza-Michael polyaddition of *prim*- or bis-*sec*-amines with bisacrylamides [13]. PAAs can be designed to be water-soluble. The polymerization typically occurs at room temperature in an aqueous medium without the need for added catalysts. As a polyaddition reaction, PAA synthesis does not produce by-products. Consequently, the PAA synthetic process is considered easily scalable and respond to numerous principles of green chemistry [14]. PAAs degrade in water under conditions of high dilution [15] and many of them are biocompatible and can find application in biotechnology [16–18]. In addition, they demonstrated no phytotoxicity

Table 2
Average charge on PAAs' repeat units.

PAA	pK_a values	IP	Net charge at pH 7.0 [a]	Positive/Negative charge [a]
M-SER	$pK_{a\text{-}COOH}$ = 2.3 $pK_{a\text{-}\ NR3}$ = 7.2	4.8	−0.38	0.62
M-GLY	$pK_{a\text{-}COOH}$ = 2.3 $pK_{a\text{-}\ NR3}$ = 8.1	5.2	−0.07	0.93
M-HIS	$pK_{a\text{-}COOH}$ = 2.1 $pK_{a\text{-}imid}$ = 5.1 $pK_{a\text{-}NR3}$ = 8.3	6.7	−0.04	0.96
M-TYR_{30}-ARG_{70}		8.1	−0.04 [b]	0.96 [b]
M-ARG	$pK_{a\text{-}COOH}$ = 2.4 $pK_{a\text{-}NR3}$ = 6.9 $pK_{a\text{-}guanidine}$ > 10	9.5	+0.47	1.47

[a] Data calculated from the charge distribution shown in Fig. 1.
[b] data obtained at pH 7.5. The pK_a values of M-TYR were approximated using those of M-SER due to the similarity in their α-amino acid pK_a values. Direct determination of the pK_a values of tyrosine in M-TYR_{30}-ARG_{70} was not possible due to solubility constraints.

in seed germination assays [19,20] and no aquatic toxicity in vivo tests conducted using zebrafish embryos (*Danio rerio*) as live animal models [21]. Recent studies have demonstrated that four PAAs, synthesized through the polyaddition of N,N'-methylenebisacrylamide with glycine, arginine, leucine, and glutamic acid, effectively stabilize cotton against UVA radiation in air [22]. Their effectiveness was attributed to the radical scavenging properties of the tertiary amine groups in their repeating units. To broaden the scope of this research, a new series of PAAs synthesized through the polyaddition of N,N'-methylenebisacrylamide with arginine (M-ARG), glycine (M-GLY), serine (M-SER), histidine (M-HIS), and an tyrosine/arginine mixture (M-TYR_{30}-ARG_{70}) were evaluated for their effectiveness in stabilizing cotton against UVA and UVB radiations. Notably, the α-amino acid residues of these PAAs exhibit varying UV-absorption properties. Additionally, the guanidine residues of M-ARG [23,24] and the imidazole residues of M-HIS [25,26] are recognized for their role as radical scavengers. This study aims to assess how this structural diversity influences the performance of PAAs as photostabilizers for the protection of cotton.

2. Experimental part

2.1. Materials

N,N'-methylenebisacrylamide (M, 99 %), arginine (ARG, 99 %), glycine (GLY, 99 %), serine (SER, 99 %), histidine (HIS, 99 %), tyrosine (TYR, 98 %), lithium hydroxide monohydrate (98 %), hydrochloric acid (HCl, 37 %), D_2O (>99.9 %) were purchased from Sigma-Aldrich (Milan, Italy) and used as received. Bleached cotton fabric (COT) with an area density of 240 g m^{-2} was purchased from Fratelli Ballesio S.r.l. (Turin, Italy).

2.2. Synthesis of polyamidoamines (PAAs)

Synthesis of M-HIS: N,N'-methylenebisacrylamide (0.51 g, 3.2 mmol), histidine (0.50 g, 3.2 mmol) and lithium hydroxide monohydrate (0.14 g, 3.2 mmol) were dissolved in 1.14 mL ultrapure water. The reaction mixture was heated to 50 °C under stirring for 9 days in the dark under nitrogen. After this time, it was diluted with ultrapure water, the pH adjusted to 7.0 with 6 M HCl. The product was retrieved by freeze-drying. All other PAAs were synthesized following the same procedure adopted for M-HIS, using the conditions shown in Table 1. Temperatures and times for the synthesis of each PAA differ due to the different amino acid reactivity.

PAA were analyzed by nuclear magnetic resonance, namely, ^1H NMR, ^{13}C NMR and Heteronuclear Single Quantum Coherence (HSQC) NMR.

2.3. Treatment of cotton fabrics with PAAs

Strips of cotton fabrics measuring 20 mm x 60 mm were dried at 100 °C for 4 min and then weighed. They were subsequently impregnated with a 6 wt. % PAA aqueous solution (300 μL) using an electronic micropipette and then dried at 100 °C for 4 min. The total dry solid add-ons (*Add-on, wt.- %*) were determined weighing each sample before (W_i) and after (W_f) the impregnation step. The add-ons were calculated using Eq. (1):

$$Add-on\% = \frac{W_f - W_i}{W_i} \times 100 \quad (1)$$

For all PAAs, the final add-on percentage was established at 6 %. Cotton fabrics treated with PAAs were labeled using the following format: COT/M-GLY denotes a cotton sample treated with M-GLY.

2.4. Accelerated tests for photodegradation of PAA-treated cotton samples

Accelerated photodegradation tests were conducted within a sealed solar chamber lined with aluminum foil. Samples of both untreated and PAA-treated cotton strips (20 mm x 60 mm) were placed on a rotating stand (250 rpm) and irradiated with a 500 W UV lamp (emission wavelength range: 280–400 nm) positioned 45 cm away from the sample holder. A 40 % relative humidity was obtained by placing a saturated potassium carbonate water solution in the chamber. Irradiation was paused every 15 min for a duration of 30 min to reduce both the

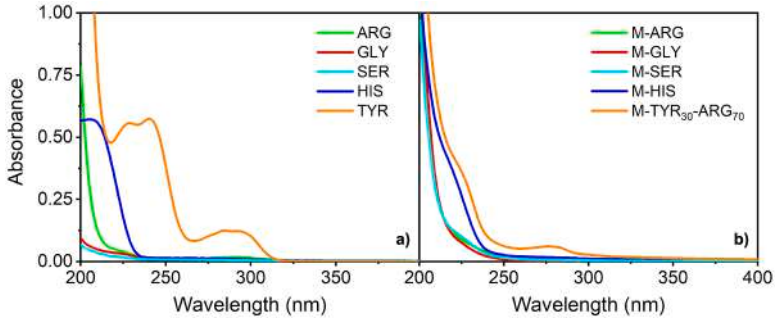

Fig. 2. UV absorption spectra of PAAs (b) and parent α-amino acids (a) recorded at concentration 0.025 mg mL^{-1} and pH 7.0, except for M-TYR_{30}-ARG_{70}, whose spectrum was recorded at pH 7.5.

Fig. 3. Digital pictures of untreated and PAA-treated cotton fabrics after 0 and 14 h photoaging (upper panel); simulated colors of photoaged cotton samples based on the determined colorimetric parameters (Section 2.5) (lower panel).

internal temperature of the chamber and the surface temperature of the samples. At the end of the irradiation cycle, the sample temperature achieved 50 °C, as measured using a Tilswall Digital thermometer (Berlin, Germany) placed at a 15 cm distance from the fabric.

After each irradiation cycle, untreated and PAA-treated cotton strips were characterized by colorimetric and FT-IR analyses. At the end of the working day, samples were stored in the dark. All tests were performed in duplicate.

At the end of the test, PAA-treated cotton fabrics were extracted with D_2O (1 mL) at room temperature for 1 h under stirring. The extracts were analyzed by ^1H NMR.

2.5. Characterization techniques

The UV absorption spectra of PAAs and their parent α-amino acids were obtained from 0.025 mg mL^{-1} water solutions at pH 7.0 using a Lambda 4 Perkin Elmer spectrophotometer (Milan, Italy) operating in the wavelength range 200–800 m, except for the M-TYR_{30}-ARG_{70} copolymer, which was analyzed at pH 7.5 due to solubility constrains.

The morphology of COT and COT/PAA samples was examined after 0 h and 14 h UV irradiation. The surface of the cotton fabrics (5 mm x 5 mm) was gold metallized and then analyzed with a Zeiss field-emission scanning electron microscope (FE-SEM), model ZEISS-SIGMA 300 operating at 8.5 mm working distance and 5 kV beam voltage (Zeiss, Ramsey, NJ, USA).

The surfaces of untreated and PAA-treated cotton strips were spectrophotometrically analyzed following the ISO11664 standard [27] using a YS3010 Handheld Spectrophotometer (3nh Global, Guangzhou, China) equipped with the SQCX software. The following CIELAB color space parameters, representing the full range of human color perception, were recorded: color change (ΔE^*), chroma (C^*), hue (h^*) described by Eq. (2)–(4):

$$\Delta E^* = \sqrt{(\Delta L^*)^2 + (\Delta a^*)^2 + (\Delta b^*)^2} \quad (2)$$

$$C^* = \sqrt{a^{*2} + b^{*2}} \quad (3)$$

$$h = arctg\frac{b^*}{a^*} \quad (4)$$

where L^* is the sample brightness ranging from 0 (black) to 100 (white), a^* (green-red axis) and b^* (blue-yellow axis) are chromaticity coordinates. Neither the chromaticity coordinates nor the resulting ΔE^* have physical units, as they are abstract quantities representing visual characteristics. ΔE^* measures color difference on a perceptual scale reflecting human color perception. Thus, a higher ΔE^* indicates greater color changes due to aging. C^* quantifies color vividness or intensity, with lower values indicating less saturation and more neutral tones, while higher values correspond to more intense, saturated colors. Hue represents the color's direction in the a^*-b^* plane and is measured in degrees. Color differences were categorized as follows: not present ($\Delta E^* = 0$); imperceptible to the human eye ($0 < \Delta E^* \leq 1$); perceptible under

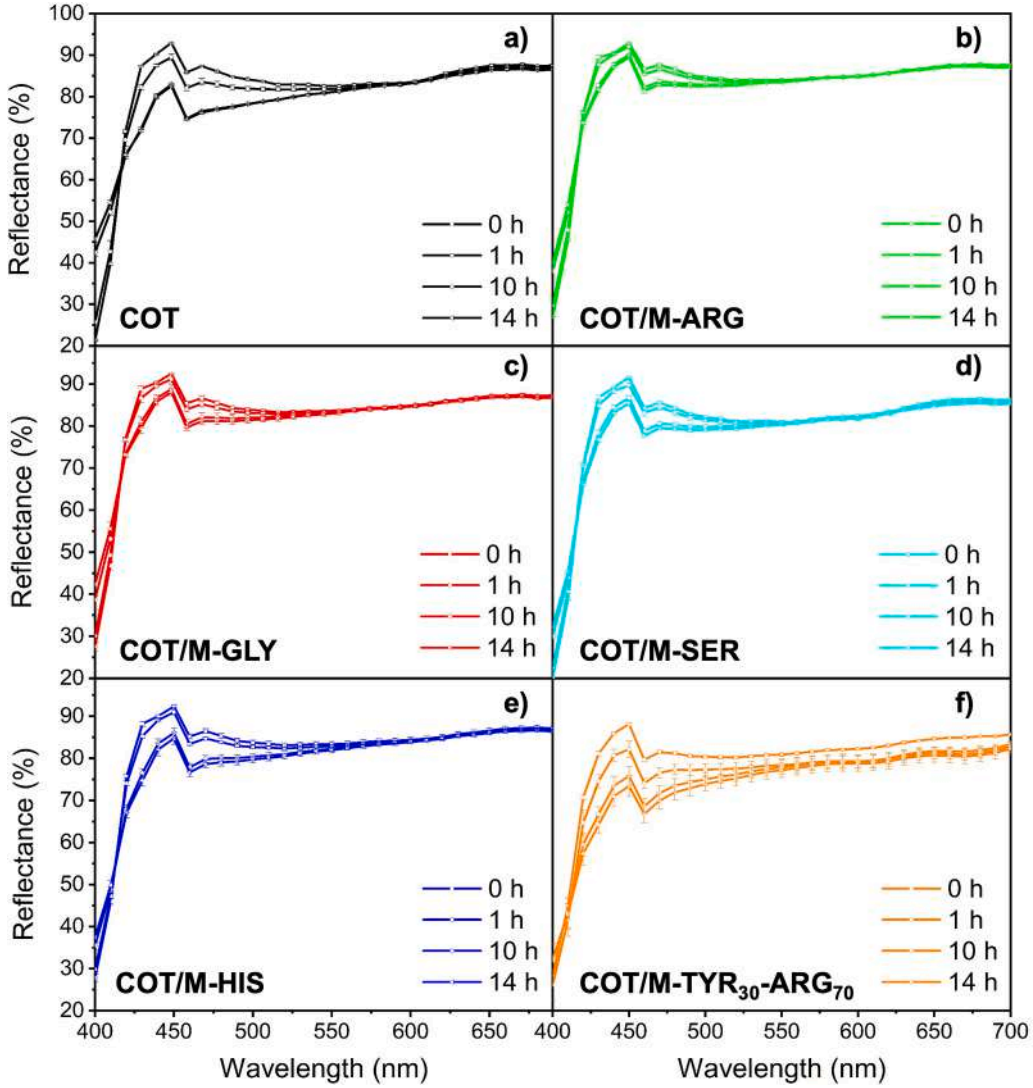

Fig. 4. Reflectance spectra of untreated and PAA-treated cotton at different photoaging stages.

close observation ($1 < \Delta E^* \leq 2$); immediately noticeable ($2 < \Delta E^* \leq 10$); highly distinct ($11 < \Delta E^* \leq 49$); and extremely distinct ($\Delta E^* \geq 50$) [28].

The X-ray diffraction (XRD) spectra of COT and COT/PAA samples were recorded using a Miniflex 600 diffractometer with Cu $K_{\alpha 1}$ radiation at 1.5405 Å, at 40 kV voltage and 15 mA current (Rigaku Europe SE, Germany).

3. Results and discussion

3.1. Synthesis, ionic species distribution and UV absorption spectra of PAAs

Five water-soluble polyamidoamines (PAAs) were investigated for their potential as photostabilizers of cotton fabrics. These PAAs were synthesized through the aza-Michael polyaddition of N,N′-methylenebisacrylamide with arginine (M-ARG), glycine (M-GLY), serine (M-SER) and histidine (M-HIS) (Scheme 1a) in a 1:1 molar ratio, and with an tyrosine/arginine mixture in a 1:0.7:0.3 molar ratio (M-TYR_{30}-ARG_{70}, Scheme 1b). The synthesis was conducted in a pH 11 aqueous solution with a 50 wt. % solid concentration and varying reaction times, to account for the differing reactivities of α-amino acids caused by the steric hindrance of their side substituents [13]. The raw products were obtained through freeze-drying without any additional purification steps. Their chemical structures of the final products were elucidated by ^{1}H NMR, ^{13}C NMR and HSQC spectroscopy (Figures S1 - S5, in Supplementary Materials). The number average molecular weights, determined by ^{1}H NMR spectroscopy, varied in the range 10,000–12,000.

PAAs derived from α-amino acids are amphoteric polyelectrolytes, whose physico-chemical properties are governed by their ionization state, which is obviously pH-dependent. The radical scavenging activity may also be influenced by the charge distribution of PAAs. In this study, the ionic species distributions of PAAs (Fig. 1) were calculated using the pK_a values of the ionizable groups in their repeating units (Figures S6–S12, Table 2), which were experimentally determined as described in the Supplementary Materials. The isoelectric points (IPs) are consistent with the presence of an overall negative charge in the repeat units of M-GLY, M-SER, M-HIS at pH 7.0, and of M-TYR_{30}-ARG_{70} at the working pH of 7.5, while M-ARG exhibits an overall positive charge under the same conditions.

The UV absorption behavior of PAAs was analyzed in this study to evaluate the potential influence of chromophores in their repeating units on their radical scavenging performance. Fig. 2 shows the UV absorption spectra of PAAs at pH 7.0, along with those of the parent α-amino acids. The spectrum of M-TYR_{30}-ARG_{70} was recorded at pH 7.5, due to solubility constraints.

All PAAs share the characteristic absorption features of the amide groups in the main chain, displaying a strong absorption band at 190–220 nm, attributed to the $\pi \rightarrow \pi$ transition of the amide C═O, and a

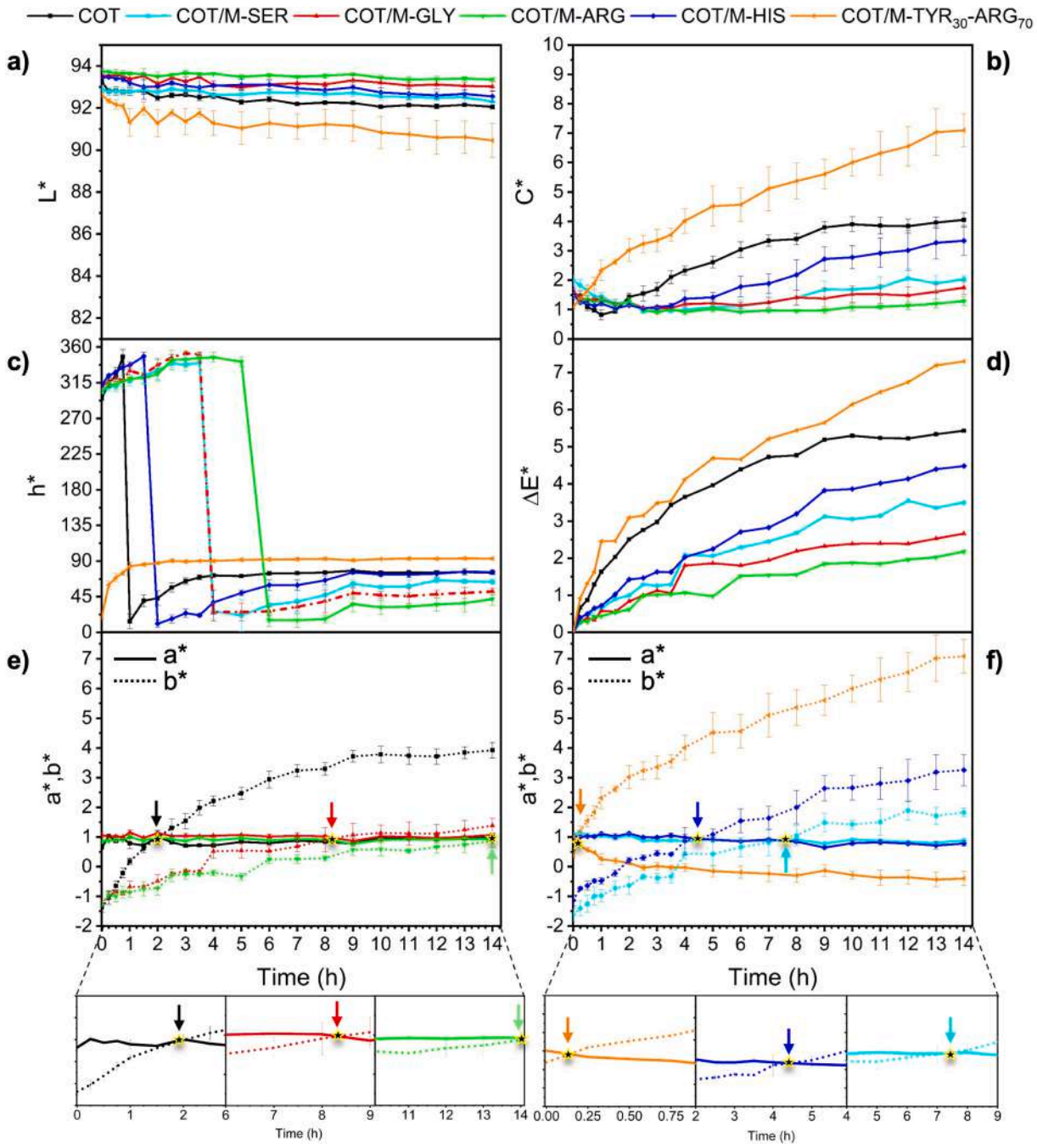

Fig. 5. Change of the color parameters of untreated and PAA-treated cotton during accelerated photoaging tests. L^* = brightness; C^* = chroma; h^* = hue; ΔE^* = color change; a^*, b^* = chromaticity coordinates. Definitions are given in Section 2.5.

weak absorption band at 210–240 nm due to the n → π transition of the amide C═O. M-GLY, M-SER, and M-ARG do not exhibit additional absorption bands, as their amino-acidic pendants absorb only in the far-UV region (<230 nm). In contrast, M-HIS and M-TYR$_{30}$-ARG$_{70}$ show absorption bands in the UVC and UVB regions, respectively, due to the presence of conjugated structures in their amino-acid pendants. More in detail, the spectrum of M-HIS shows a strong absorption band in the 200–230 range due to the π → π transition of the aromatic system of the imidazole ring, as well as a weak absorption band at 250–280 nm due to the n → π transition of the imidazole ring. Finally, the spectrum of M-TYR$_{30}$-AG$_{70}$ shows a strong absorption at 190–230 nm, due to the π → π* transitions in the benzene ring and a weaker absorption at 270–280 nm due to the *n* → *π* transition of the lone pair (n) electrons on oxygen to π* transitions.

3.2. Photoaging tests

Accelerated photoaging tests were conducted on cotton fabrics with a 6 % PAA add-on. PAA-treated cotton strips were exposed to UV irradiation in the 280 - 400 nm wavelength range in air, at 30–35 °C and 40 % relative humidity. The irradiation cycles lasted 15 min, followed by a 30-min rest period during which analyses were conducted to monitor any structural and color changes in the samples by recording the FT-IR and reflectance spectra in the UV–VIS range. The reflectance spectra were recorded on fabrics aligned along the same axis. At the end of the workday, cotton samples were stored in darkness. Samples were exposed to UV irradiation for a total duration of 14 h. Fig. 3 shows comparative images of untreated and PAA-treated cotton strips taken before and after aging. As evident from the simulated colors, the COT/PAA samples

Table 3
Colorimetric parameters of photoaged cotton samples.

	Maximum reflectance reduction at 14 h (%)	$b^*_{14\ h}$	$\Delta b^*_{14\ h}$	$t_{hue\ drop}$ [a] (h)	$t_{crossover}$ [b] (h)	$\Delta E^*_{14\ h}$
COT	11	3.9 ± 0.3	5.3	1	2	5.4
COT/M-ARG	4	0.9 ± 0.2	2.1	6	14	2.2
COT/M-GLY	5	1.4 ± 0.3	2.6	4	8.5	2.7
COT/M-SER	7	1.8 ± 0.1	3.5	4	7.5	3.5
COT/M-HIS	8	3.3 ± 0.5	4.4	2	4.5	4.5
COT/M-TYR_{30}-ARG_{70}	17	7.1 ± 0.6	6.8	0.25	0.25	7.3

[a] Time at which a sudden decrease of h^* is observed, corresponding to the sign change of the b^* coordinate.
[b] Time at which the a^* and b^* curves intersect.

showed no significant color difference from native cotton, except for COT/M-TYR_{30}-ARG_{70}. Following 14 h of irradiation, noticeable yellowing was observed in virgin cotton (COT). In contrast, COT/PAA samples exhibited substantially less yellowing, except for COT/M-TYR_{30}-ARG_{70}, which showed discoloration similar to that of photoaged cotton.

Notably, the FT-IR spectra of the PAA-treated cotton fabrics showed no substantial variations after 14 h irradiation (Figures S13), indicating the absence of significant structural changes during photoaging under the adopted experimental conditions.

Representative results of the spectrophotometric measurements after different irradiation times (namely, 0, 1 10 and 14 h) are shown in Fig. 4. A substantial decrease in the maximum reflectance of cotton at 450 nm was observed during the irradiation experiment. The reflectance curve stabilized after 9 h, and by 14 h, the overall reduction reached 11 %. The maximum reflectance values of COT/PAA samples, observed at 450 nm, declined at a significantly slower rate than virgin cotton, showing a reduction of only 4 %, 5 %, 7 %, 8 % for COT/M-ARG, COT/M-GLY, COT/M-SER, COT/M-HIS, respectively, and of 17 % for COT/COT/M-TYR_{30}-ARG_{70}, after 14 h of irradiation. Among all samples analyzed, only COT/M-TYR_{30}-ARG_{70} exhibited more intense coloration than virgin cotton (Fig. 3), as indicated by the maximum reflectance value decreasing by 17 % comparing to 11 % for cotton. This analysis allowed the cotton samples to be ranked according to their resistance to photoaging, as follows: COT/M-ARG > COT/M-GLY > COT/M-SER > COT/M-HIS > COT> COT/M-TYR_{30}-ARG_{70}.

The color changes of photoaged cotton were better defined through monitoring the CIELAB color space parameters ΔE^* (color change), C^* (chroma), L^* (brightness), and the chromatic coordinates a^* (green – red axis), b^* (blue – yellow axis) and hue, h^*, defined according to Eq. (2)–(4) (Section 2.5). In practical terms, an ideal pure white has $L^* = 100$, $a^* = 0$, $b^* = 0$, and $C^* = 0$.

The results collected for both untreated- and PAA-treated cotton fabrics are shown in Fig. 5 and Table 3. In almost all case studied, the L^* value showed only a slight decrease throughout the irradiation period, with a slightly more pronounced decline for COT/M-TYR_{30}-ARG_{70} (Fig. 5a). A similar trend was observed for the a^* chromaticity coordinate in both virgin cotton and all PAA-coated cotton fabrics, except for COT/M-TYR_{30}-ARG_{70}, which exhibited a linear decrease during the first 3 h-irradiation, followed by a stable value for the remainder of the photoaging test. (Fig. 5e and f). A distinct pattern was observed for the b^* chromaticity coordinate, whose positive values indicate yellowness. In virgin cotton, the b^* value rapidly rose from −1.37 to +3.9 throughout the irradiation period, demonstrating pronounced and consistent yellowing as exposure time increased (Fig. 5e and f). However, after 9 h-irradiation, the increase in yellowness slowed significantly, and b^* remained nearly constant. In the COT/PAA samples, the b^* coordinate increased almost linearly and at a slower rate comparing to untreated cotton for all samples apart from COT/M-TYR_{30}-ARG_{70}. The maximum detected b^* values were 0.9, 1.4, 1.8, 3.3 and 7.1 for COT/M-ARG, COT/M-GLY, COT/M-SER, and COT/M-HIS respectively, corresponding to Δb^* values with respect to the non-irradiated samples ranging from 2.1 to 4.4 in the series, to be compared with Δb^* values of 5.3 and 6.8 for non-treated cotton and COT/M-TYR_{30}-ARG_{70}, respectively. Overall, similar trends as the b^* were observed for the C^* (Fig. 5b) and ΔE^* (Fig. 5d) parameters.

Interestingly, two distinct nodal points can be identified to classify the efficacy of photostabilizers: (1) the steep drop in the h^* parameter (Fig. 5c), linked to the sign change of the b^* coordinate, and (2) the crossover point of the a^* and b^* curves (Fig. 5e and f and inlets). The latter marks a shift in the relative contribution of chromaticity coordinates, where $b^*/a^* > 1$ indicates the increasing dominance of the yellow color component. The crossover point coincides with the moment when h^* reaches 45°, corresponding to $\arctan(b^*/a^*) = 1$ (Fig. 5c). Finally, the ΔE^* value (Fig. 5d), indicating the total color change, proved a useful parameter to quantify the effect of the photoaging on untreated and PAA-treated cotton fabrics.

Based on the analysis of the colorimetric parameters reported in Table 3, the effectiveness of PAA photostabilizers can be ranked as follows: M-ARG > *M*-GLY > *M*-SER > *M*-HIS > *M*-TYR_{30}-ARG_{70}. A clear gap in efficacy is observed between the top three polymers and the remaining ones. Notably, COT/M-TYR_{30}-ARG_{70} consistently performed worse than untreated cotton.

3.3. Efficacy of PAAs as photostabilizers for cotton

The photostabilizing effectiveness of PAA coatings on cotton can be attributed to multiple factors. An essential factor is their stability under UV irradiation, which depends on the ability to establish deexcitation pathways that enable rapid internal conversion to the electronic ground state, along with intramolecular vibrational redistribution and cooling that occur faster than dissociation. Another crucial factor is their antioxidant properties and radical-scavenging activity. Scavengers react with reactive oxygen species (ROS) generated during cellulose photooxidation, effectively blocking them and preventing further oxidation [29]. The PAAs analyzed in this study share key structural features, including two amide groups and a tertiary amine in the backbone, as well as a carboxyl group in the side chain. While both amide and carboxyl functions are generally stable against radical reactions and oxidation, the radical scavenging capacity of M-ARG, M-GLY, M-SER and M-HIS is attributed to the tertiary amine groups in the main chain, which donate their lone electron pairs to react with radicals, forming less reactive species [30]. Notably, at the working pH of 7.0, a well-defined percentage of the tertiary amines in the PAA backbones are deprotonated, namely 53 %, 7 %, 38 %, and 5 % for M-ARG, M-GLY, M-SER and M-HIS, respectively (Fig. 1).

The differing effectiveness of PAAs in protecting cotton from photoaging is clearly associated with the nature of the lateral pendants derived from α-amino acid residues, which influence the stability of the entire macromolecular structure.

PAAs with UV-absorbing lateral groups, specifically M-HIS (absorbing in the UVC range) and M-TYR_{30}-ARG_{70} (absorbing in the UVB range), are the most vulnerable. The latter failed to protect cotton from photoaging. As above stated, the vulnerability to UV radiation is

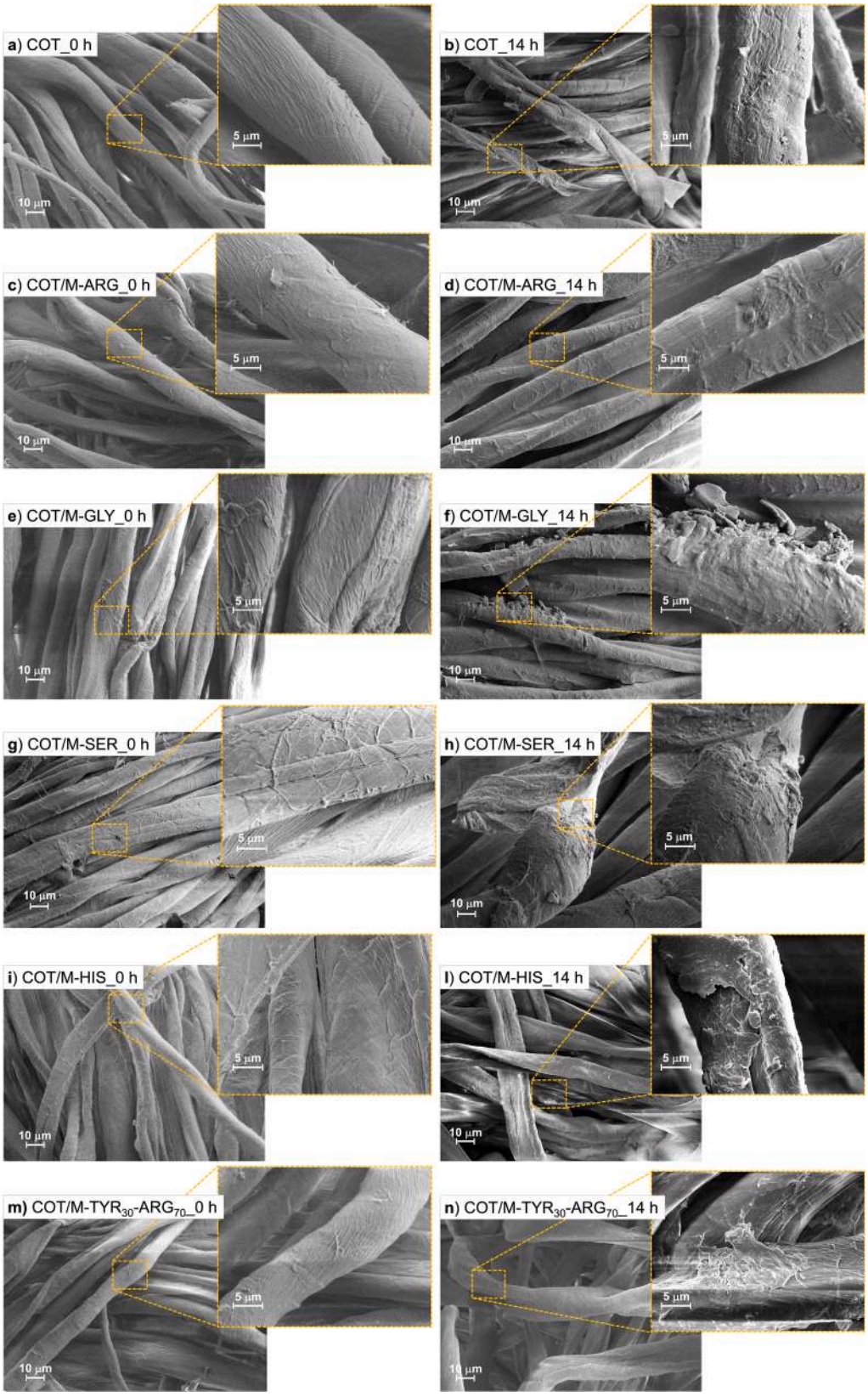

Fig. 6. FE-SEM micrographs in secondary electron mode (2500X) of untreated cotton (COT) and cotton fabrics treated with 6 % add-on M-ARG, M-GLY, M-SER, M-HIS, and M-TYR_{30}-ARG_{70} after 0 h (a, c, e, g, i and m) and 14 h UV irradiation (b, d, f, h, l and n). Insert magnification: 10000X.

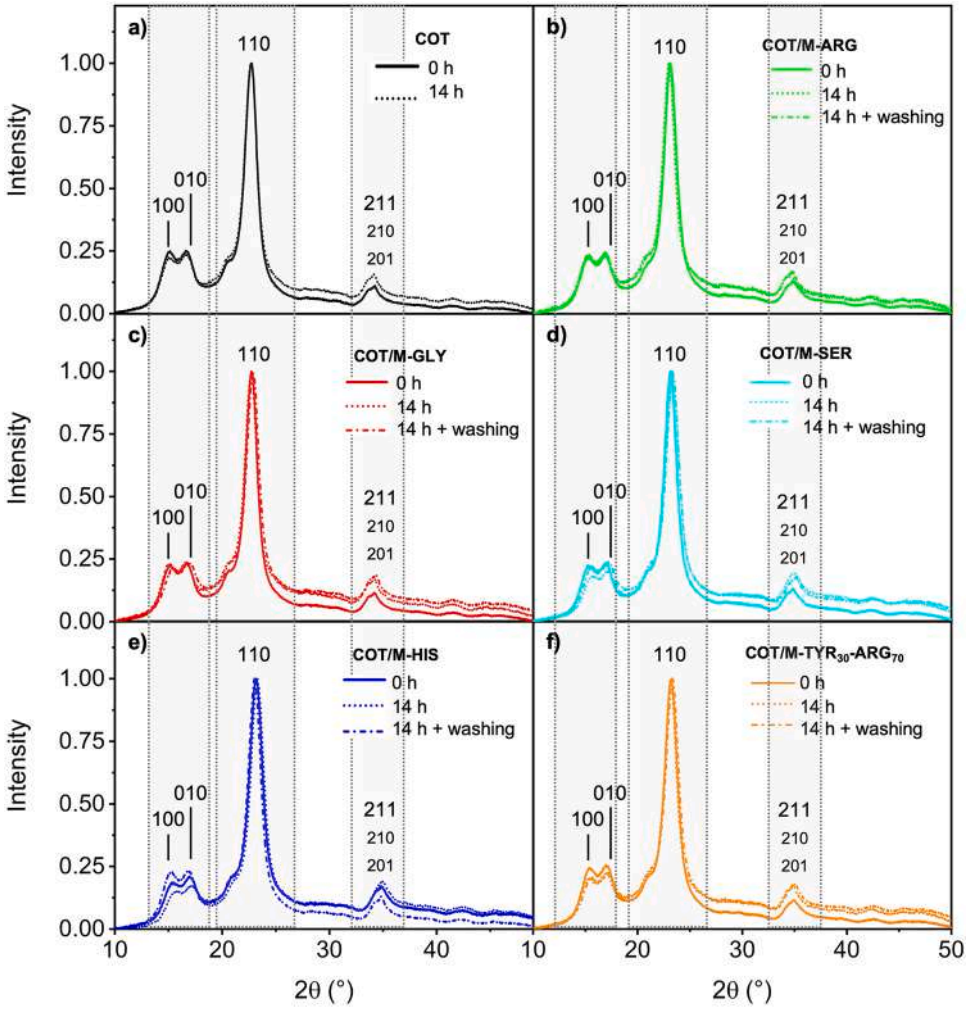

Fig. 7. XRD spectra of untreated cotton (COT, a) and cotton fabrics treated with 6 % add-on M-ARG (b), M-GLY (c), M-SER (d), M-HIS (e), and M-TYR_{30}-ARG_{70} (f) after 0 and 14 h irradiation and after washing with water at the end of irradiation.

Table 4
Position of XRD signals and crystallographic parameters of photoaged cotton samples.

Sample	2θ			d (nm)		
Assignment	100	010	110	100	010	110
COT	15.19	16.73	23.08	0.294	0.268	0.196
COT/M-ARG	15.25	16.82	23.09	0.293	0.266	0.196
COT/M-GLY	15.25	16.80	23.08	0.293	0.266	0.196
COT/M-SER	15.33	17.00	23.27	0.291	0.263	0.195
COT/M-HIS	15.24	16.88	23.23	0.293	0.265	0.195
COT/M-TYR30-ARG70	15.40	17.00	23.27	0.290	0.263	0.195

linked to the ability to dissipate the absorbed energy. Radical generation after dissociation is enhanced by stabilization through the resonance of the imidazole residues in M-HIS and the tyrosine residue in M-TYR. PAAs lacking chromophores in the side chains (M-ARG, M-GLY and M-SER) are intrinsically photostable. The superior stability of M-GLY compared to M-SER is due to the absence, in the former, of tertiary hydrogens, which are relatively susceptible to radical reactions. Finally, M-ARG's exceptional performance is due to its guanidine residues, which engage in electron transfer reactions with radicals, forming radical cations.

3.4. Morphological analysis of PAA-impregnated cotton specimens

Field-emission scanning electron microscopy (FE-SEM) was used to examine the impact of UV irradiation on the surface morphology of both untreated and PAA-treated cotton fabrics. Cotton fibers display the characteristic elongated, ribbon-like shape with natural twists of the virgin material and feature a flat, smooth surface (Fig. 6a) [31]. The cellulose microfibrils that form the primary wall of cotton fibers are visible at maximum magnification (10000X, insert in Fig. 6a). Occasionally, inhomogeneities due to their natural origin can be observed.

The morphology of all PAA-treated cotton samples is nearly identical, irrespective of the PAA type. Due to the hydrophilic nature of both PAAs and cotton, a thin, continuous, and homogeneous coating was formed on the fabric's surface. However, PAAs not only cover the fiber surfaces but also infiltrate the cotton weft, extending to the microfibrils. This is clearly illustrated in Figs. 6a, c, e, g, i, and m, as well as in the inserts at 10000X. This deep penetration enhances the PAAs' ability to protect cellulose from photooxidation, as it creates a direct and intimate contact between cellulose fibers and photostabilizer.

After 14 h UV exposure, the morphology of the cotton fibers showed noticeable changes, with structural defects caused by surface erosion observed in several areas of the sample, as seen in the insert of Fig. 6b In contrast, when PAA was present, no such effect occurred, and the fibers remained intact and uniformly coated. The only noticeable difference, at least in COT/M-GLY, COT/SER, COT/M-HIS, and COT/M-TYR_{30}-ARG_{70} samples, was the occasional presence of cracks and partial delamination

Table 5
Colorimetric parameters of photoaged COT/PAA samples after washing with water.

	L*	a*	b*	ΔE* [a]	Simulated colors [b]
COT_{t0} [c]	93.3 ± 0.1	0.65 ± 0.02	-1.37 ± 0.15	-	
Post extraction					
COT/M-ARG	93.4 ± 0.2	0.98 ± 0.09	0.44 ± 0.09	1.8	
COT/M-GLY	93.1 ± 0.1	1.09 ± 0.02	0.95 ± 0.15	2.4	
COT/M-SER	92.8 ± 0.1	0.92 ± 0.04	0.63 ± 0.13	2.1	
COT/M-HIS	92.5 ± 0.6	1.04 ± 0.20	1.93 ± 0.52	3.4	
COT/M-TYR_{30}-ARG_{70}	90.7 ± 0.3	0.88 ± 0.21	3.97 ± 0.48	5.9	

[a] Color change with respect to virgin cotton before irradiation.
[b] simulated colors of photoaged cotton samples after water extraction based on the determined colorimetric parameters.
[c] virgin cotton.

(Figs. 6f, h, n, and inserts). However, no such damage was observed in the COT/M-ARG samples, where the coating was intact and crack-free (Fig. 6d).

3.5. Effect of photoaging on the crystallinity of untreated and PAA-treated cotton fabrics

X-ray diffraction (XRD) analysis was used to investigate the impact of photoaging on the crystalline structure integrity of cellulose in both untreated and PAA-treated cotton samples. Fig. 7 presents the XRD patterns of these samples obtained before and after 14 h of irradiation, as well as those obtained after the extraction of PAAs at the conclusion of the photoaging experiments. The cellulose crystallinity parameters obtained from spectra run before irradiation are shown in Table 4. The X-ray diffraction spectrum of cellulose in untreated cotton before irradiation exhibits characteristic strong and broad diffraction peaks at 15.19°, 16.73° and 23.08°, corresponding to the (100), (010), (110) crystal facets of cellulose. Additionally, a shoulder around 20° is attributed to the (012)/(102) facets, while a less intense broad peak centered at 35.10° corresponds to the (2–1–1)/(210)/(201) crystal facets [32,33]. Meanwhile, the degree of crystallinity of cellulose remained largely unchanged.

3.6. Analysis of cotton fabrics and PAA coatings after 14 h UV irradiation

At the conclusion of the photoaging tests, deuterated water was used to extract the PAA coatings from the impregnated cotton strips. The PAA solutions obtained were analyzed via ^{1}H NMR. The spectra of photoaged PAAs (Figures S1d-S5d) were nearly identical to those of native PAAs before irradiation. This confirms that no degradation occurred, and no cellulose decomposition residues were extracted.

The washed cotton strips were analyzed by reflectance spectrophotometry. The colorimetric parameters determined (Table 5) indicate that after PAA removal, cotton deriving from COT/M-ARG, COT/M-GLY and COT/M-SER largely regained their original color, although not completely. Specifically, the ΔE^* values, calculated using cotton as a reference, ranged between 1.7 and 2.2, indicating minimal color changes perceptible to the naked eye, as clearly demonstrated by the simulated colors in the table. The color deviation from original cotton was more pronounced in cotton samples deriving from COT/HIS and COT/M-TYR_{30}-ARG_{70}, as reflected by their respective ΔE^* values of 3.2 and 4.2.

4. Conclusions

A set of α-amino acid-derived polyamidoamines - M-ARG, M-GLY, M-SER, M-HIS, and M-TYR_{30}-ARG_{70} - was examined for their potential as photostabilizers for cotton fabric. Some polymers in this family have been shown to protect cotton from photoaging, likely by scavenging free radicals. Among PAAs studied here, M-HIS and M-TYR_{30}-ARG_{70} absorbed radiations in the UVC and UVB wavelength range, respectively, while the others absorbed only in the far UV. One of the primary goals of this research was indeed to determine whether UV-absorbing chromophores influence their effectiveness as radical scavengers.

To evaluate photoaging, untreated and 6 % PAA-treated cotton strips were irradiated with UVA and UVB light in a solar chamber featuring reflective surfaces. All samples underwent 15-minute irradiation cycles, followed by retrieval and analysis using FT-IR spectroscopy and colorimetric tests, for a total duration of 14 h. As expected, virgin cotton exhibited progressive yellowing, which appeared more pronounced than that observed following PAA treatments, except for M-TYR_{30}-ARG_{70}. However, FT-IR analysis did not reveal any structural changes on the cotton surface during irradiation, regardless of the presence of PAA.

Colorimetric parameters were used to rank the efficacy of the PAA photostabilizers as follows: M-ARG > *M*-GLY > *M*-SER > *M*-HIS > *M*-TYR_{30}-ARG_{70}. Only the COT/M-TYR_{30}-ARG_{70} samples photodegraded to a larger extent than virgin cotton.

Morphological analysis revealed meaningful insights. FE-SEM analysis showed that PAAs formed a uniform and continuous coating on the cotton fibers. Previous studies have indeed shown that PAAs penetrate deeply into the cotton threads, facilitated by their high hydrophilicity, which enables close interaction between cotton fibrils and PAAs. After photoaging, the PAA coatings occasionally developed wrinkles and surface fractures, suggesting localized embrittlement. This structural degradation accounted for the reduced shielding effectiveness of the coatings against UV irradiation. At the end of the photoaging tests, PAAs were extracted from the aged PAA-treated cotton fabrics using deuterated water and analyzed by ^{1}H NMR spectrometry. Spectral analysis revealed no significant structural changes caused by UV exposure. Meanwhile, the extracted cotton strips from COT/M-ARG, COT/M-GLY, and COT/M-SER largely recovered their original whiteness, whereas those from COT/M-HIS and COT/M-TYR_{30}-ARG_{70} exhibited residual yellowing.

The photostabilizing effectiveness of α-amino acid-derived PAA coatings on cotton results from multiple factors. The least effective PAAs were those bearing UV absorbing aromatic or heteroaromatic groups in the side chains (M-HIS and M-TYR_{30}-ARG_{70}) due to the structural destabilization deriving from the mobility of the α-hydrogens in radical

reactions. PAAs lacking chromophores in the side chains (M-ARG, M-GLY and M-SER) are intrinsically photostable. Their effectiveness can be ascribed to the radical scavenging activity of the tertiary amine groups in the main chain. The superior stability of M-GLY compared to M-SER is due to the absence, in the former, of tertiary hydrogens, which are relatively susceptible to radical reactions. Finally, the exceptional performance of M-ARG is ascribed to its guanidine residues, which engage in electron transfer reactions with radicals, forming radical cations.

Overall, these findings confirm the potential of α-amino acid-derived PAAs as anti-photoaging additives for cotton, especially those with side residues possessing radical scavenging ability, such as the guanidine residue. This highlights the importance of thoroughly studying the interaction of radicals with PAAs containing differently arranged guanidine residues in their repeat units.

Funding

This research was funded by Università degli Studi di Milano, Piano di Sostegno alla Ricerca 2023 – linea 2, grant number PSR2023_DIP_005_PI_JALON.

CRediT authorship contribution statement

Sofia Treccani: Methodology, Investigation. **Jenny Alongi:** Writing – original draft, Funding acquisition, Conceptualization. **Paolo Ferruti:** Writing – review & editing, Conceptualization. **Elisabetta Ranucci:** Writing – review & editing, Writing – original draft, Supervision, Conceptualization.

Declaration of competing interest

The authors declare that they have no known competing financial interests or personal relationships that could have appeared to influence the work reported in this paper.

Supplementary materials

Supplementary material associated with this article can be found, in the online version, at doi:10.1016/j.polymdegradstab.2025.111430.

Data availability

The data that has been used is confidential.

References

[1] J. Malešič, J. Kolar, M. Strlič, D. Kočar, D. Fromageot, J. Lemaire, O. Haillant, Photo-induced degradation of cellulose, Polym. Degrad. Stabil. 89 (2005) 64–69, https://doi.org/10.1016/j.polymdegradstab.2005.01.003.
[2] A. Merlin, J. Fouassier, Photochemical investigations into cellulosic materials I. Free radical generation in cellulose by photosensitized excitation, Angew. Makromol. Chem. 86 (1980) 109–121, https://doi.org/10.1002/apmc.1980.050860108.
[3] V. Vosmansk, R.A. Barb, K. Kolařova, S. Rimpelov, J. Heitz J, Effect of VUV-excimer lamp treatment on cellulose fiber, Int. J. Polym. Anal. Charact. 21 (2016) 337–347, https://doi.org/10.1080/1023666X.2016.1156897.
[4] D.N.-S. Hon, Photooxidative degradation of cellulose: reactions of the cellulosic free radicals with oxygen, J. Polym. Sci. Polym. Chem. Ed. 17 (1979) 441–454, https://doi.org/10.1002/pol.1979.170170214.
[5] J. Kolar, Mechanism of autoxidative degradation of cellulose, Restaurator (1997) 163–176.
[6] R. Hiatt, T. Mill, F.R. Mayo, Homolytic decompositions of hydroperoxides. i. summary and implications for autoxidation, J. Org. Chem. 33 (1968) 1416–1420, https://doi.org/10.1021/jo01268a022.
[7] J.L. Hodgson, M.L. Coote, M.L. Coote, Clarifying the mechanism of the denisov cycle: how do hindered amine light stabilizers protect polymer coatings from photo-oxidative degradation? Macromolecules 43 (2010) 4573–4583, https://doi.org/10.1021/ma100453d.
[8] Y.-N. Yao, Y. Wang, H. Zhang, Y. Gao, T. Zhang, K. Kannan, A review of sources, pathways, and toxic effects of human exposure to benzophenone ultraviolet light filters, Eco-Environ. Health 3 (2024) 30–44, https://doi.org/10.1016/j.eehl.2023.10.001.
[9] J.F. Mao, W. Li, C.N. Ong, Y. He, M.-C. Jong, K.Y.-H. Gin, Assessment of human exposure to benzophenone-type UV filters: a review, Environ. Int. 167 (2022) 107405, https://doi.org/10.1016/j.envint.2022.107405.
[10] Z.-Q. Shi, Y.-S. Liu, Q. Xiong, W.W. Cai, G.-G. Ying, Occurrence and risk assessment of benzothiazole, benzotriazole and benzenesulfonamide derivatives in airborne particulate matter from an industrial area in Spain, Sci. Tot. Environ. 708 (2020) 135065, https://doi.org/10.1016/j.scitotenv.2019.135065.
[11] H. Zhou, X. Hu, M. Liu, D. Yin, Benzotriazole ultraviolet stabilizers in the environment: a review of analytical methods, occurrence, and human health impacts, TrAC Trends Anal. Chem. 166 (2023) 117170, https://doi.org/10.1016/j.trac.2023.117170.
[12] Y. Zhao, Y. Dan, Synthesis and characterization of a polymerizable benzophenone derivative and its application in styrenic polymers as UV-stabilizer, Eur. Polym. J. 43 (2007) 4541–4551, https://doi.org/10.1016/j.eurpolymj.2007.07.029.
[13] E. Ranucci, A. Manfredi, Polyamidoamines: versatile bioactive polymers with potential for biotechnological applications, Chem. Afr. 2 (2019) 167–193, https://doi.org/10.1007/s42250-019-00046-1.
[14] M.A. Dubé, S. Salehpour, Applying the principles of green chemistry to polymer production technology, Macromol. React. Eng. 8 (2014) 7–28, https://doi.org/10.1002/mren.201300103.
[15] M. Arioli, A. Manfredi, J. Alongi, P. Ferruti, E. Ranucci, Highlight on the mechanism of linear polyamidoamine degradation in water, Polymers 12 (2020) 1–16, https://doi.org/10.3390/polym12061376.
[16] R. Cavalli, L. Primo, R. Sessa, G. Chiaverina, L. di Blasio, J. Alongi, A. Manfredi, E. Ranucci, P. Ferruti, The AGMA1 polyamidoamine mediates the efficient delivery of SiRNA, J. Drug Target. 25 (2017) 891–898, https://doi.org/10.1080/1061186X.2017.1363215.
[17] M. Argenziano, C. Dianzani, B. Ferrara, S. Swaminathan, A. Manfredi, E. Ranucci, R. Cavalli, P. Ferruti, Cyclodextrin-based nanohydrogels containing polyamidoamine units: a new dexamethasone delivery system for inflammatory diseases, Gels 3 (2017) 22, https://doi.org/10.3390/gels3020022.
[18] L. Mascheroni, M.V. Dozzi, E. Ranucci, P. Ferruti, V. Francia, A. Salvati, D. Maggioni, Tuning polyamidoamine design to increase uptake and efficacy of ruthenium complexes for photodynamic therapy, Chem 58 (2019) 14586–145994, https://doi.org/10.1021/acs.inorgchem.9b02245.
[19] J. Alongi, A. Costantini, P. Ferruti, E. Ranucci, Evaluation of the eco-compatibility of polyamidoamines by means of seed germination test, Polym. Degrad. Stab. 167 (2022) 109854, https://doi.org/10.1016/j.polymdegradstab.2022.109854.
[20] E. Ranucci, S. Treccani, P. Ferruti, J. Alongi, The seed germination test as a valuable tool for the short-term phytotoxicity screening of water-soluble polyamidoamines, Polymers 16 (2024) 1744, https://doi.org/10.3390/polym16121744.
[21] S. Treccani, P. Ferruti, J. Alongi, E. Monti, D. Zizioli, E. Ranucci, Ecotoxicity assessment of α-amino acid-derived polyamidoamines using zebrafish as a vertebrate model, Polymers 16 (2024) 2087, https://doi.org/10.3390/polym16142087.
[22] J. Alongi, S. Treccani, V. Comite, P. Fermo, P. Ferruti, E. Ranucci, Polyamidoamine-based photostabilizers for cotton fabrics, Polym. Degrad. Stabil. 228 (2024) 110938, https://doi.org/10.1016/j.polymdegradstab.2024.110938.
[23] G. Yildiz, A.T. Demiryürek, I. Sahin-Erdemli, I. Kanzik, Comparison of antioxidant activities of aminoguanidine, methylguanidine and guanidine by luminol-enhanced chemiluminescence, Br. J. Pharmacol. 124 (1998) 905–910, https://doi.org/10.1038/sj.bjp.0701924.
[24] Y.-X. Wang, W.-C. Su, Q. Wang, Y.-F. Lin, Y. Zhou, L.-F. Lin, S. Ren, Y.-T. Li, Q.-X. Chen, Y. Shi, Antityrosinase and antioxidant activities of guanidine compounds and effect of guanylthiourea on melanogenesis, Process. Biochem. 85 (2019) 84–96, https://doi.org/10.1016/j.procbio.2019.07.003.
[25] T. Nauser, A. Carreras, Carbon-centered radicals add reversibly to histidine-implications, Chem. Commun. 50 (2014) 14349, https://doi.org/10.1039/C4CC05316H.
[26] Z. Zhao, C. Fu, Y. Zhang, A. Fu, Dimeric histidine as a novel free radical scavenger alleviates non-alcoholic liver injury, Antioxidants 10 (2021) 1529, https://doi.org/10.3390/antiox10101529.
[27] ISO 2469 Paper, Board and Pulps - Measurement of Diffuse Radiance Factor (diffuse reflectance Factor), International Organization for Standardization, Geneve, 2024.
[28] G.Z. Schuessler. https://zschuessler.github.io/DeltaE/learn/, 2024.
[29] M. Jablonsky, J. Sima, Oxidative degradation of paper - A mini review, J. Cult. Herit. 48 (2021) 269–276, https://doi.org/10.1016/j.culher.2021.01.014.
[30] R. Davand, M.R. Rahimpour, S. Hassanajili, R. Rashedi, Theoretical and experimental assessment of UV resistance of high-density polyethylene: screening and optimization of hindered amine light stabilizers, J. Appl. Polym. Sci. 138 (2021) 51262, https://doi.org/10.1002/app.51262.
[31] C. Vigneswaran, M. Ananthasubramanian, P. Kandhavadivu, Bioprocessing of natural fibres. Bioprocessing of Textiles Fundamentals For Applications and Research Perspective, Woodhead Publishing India PVT. LTD, 2014, pp. 53–188, https://doi.org/10.1016/B978-93-80308-42-5.50003-2.
[32] A.D. French, Idealized powder diffraction patterns for cellulose polymorphs, Cellulose 21 (2014) 885–896, https://doi.org/10.1007/s10570-013-0030-4.
[33] H. Zhao, J.H. Kwak, Z.C. Zhang, H.M. Brown, B.W. Arey, J.E. Holladay, Studying cellulose fiber structure by SEM, XRD, NMR and acid hydrolysis, Carbohydr. Polym. 68 (2007) 235–241, https://doi.org/10.1016/j.carbpol.2006.12.013.